

## Anomalous transmission of x rays scattered by phonons through germanium crystals: A high-angular-resolution study

Masahiro Mori, Yasuji Kashiwase, Motokazu Kogiso, Katsutoshi Ushida, and Masayuki Minoura  
*Department of Physics, College of General Education, Nagoya University, Chikusa, Nagoya 464-01, Japan*

Tetsuya Ishikawa\* and Satoshi Sasaki†

*Photon Factory, National Laboratory for High Energy Physics, Tsukuba, Ibaraki 305, Japan*

(Received 4 September 1991)

An intensity-profile analysis has clarified the origin of a sharp diffraction line which has been observed in the  $220$  thermal diffuse scattering from a thick perfect germanium crystal oriented in a direction offset by the Bragg angle in the transmission geometry. Experimental intensity measurements were performed with monochromatic synchrotron radiation, with use of a high-angular-resolution diffractometry system. The dependence of the intensity profiles on the crystal thickness and orientation was investigated in detail. A theoretical analysis of the intensity profiles was made on the basis of the dynamical diffraction theory including absorption and the kinematical theory of thermal diffuse scattering. We show that the diffraction peak is caused by dynamical Bragg reflection and anomalous transmission of x rays following thermal diffuse scattering in the absorbing perfect crystal and a satisfactory agreement is obtained between the experimental intensity peak profile and the calculated one. These results lend further support to our earlier interpretation [Y. Kashiwase *et al.*, *Phys. Rev. Lett.* **62**, 925 (1989)].

### I. INTRODUCTION

Diffraction lines, which appear as an intensity excess or deficit depending on experimental conditions, have been observed recently in thermal diffuse scattering (TDS) of x rays.<sup>1-3,5,6,8-15</sup> These could be explained as an effect of Bragg reflection subsequent to TDS in crystals. The diffraction lines due to TDS have the following characteristics: (1) The x-ray scattering by phonons is quasielastic and depends strongly on the crystal orientation; (2) the appearance of the diffraction lines depends on the degree of perfection of the crystal.

With mosaic crystals, deficit diffraction lines were also observed across the TDS spots in the vicinity of the reciprocal-lattice points of crystals such as urea nitrate,<sup>1</sup> pyrolytic graphite,<sup>1</sup> and LiF.<sup>2</sup> Lately, Bushuev *et al.*<sup>2,3</sup> developed a diffraction theory of inelastically scattered x rays including TDS in practical mosaic crystals on the basis of the theory<sup>4</sup> of secondary extinction. They have shown that the contrast and angular width of the deficit diffraction line depend on the degree of perfection of the mosaic crystals and compared the experimental results for LiF with theory. By applying their theory, the contrast and width of the deficit diffraction line was then quantitatively explained in the TDS from pentaerythritol<sup>5</sup> and disordered Cu-Al (Ref. 6) crystals.

In the Laue (transmission) -geometry study of perfect crystals, the dynamical diffraction pattern of TDS x rays in a crystal was predicted to be similar to Kikuchi lines and bands in electron diffraction.<sup>7</sup> An experimental study of the x-ray-diffraction pattern, however, was not made for a long time because of the very weak intensity and narrow reflection width. Excess diffraction lines in TDS patterns were finally observed on x-ray-diffraction

photographs of calcite and germanium crystals using a conventional x-ray tube.<sup>8</sup> Such excess diffraction lines were further observed photographically with monochromatized x rays of synchrotron radiation. These lines could be attributed to dynamical Bragg reflection and absorption of x rays subsequent to TDS in crystals.<sup>9</sup> In the theoretical prediction,<sup>10</sup> diffraction lines appear as excess, excess-deficit, or deficit lines according to the level of x-ray absorption in a perfect crystal. A pair of excess diffraction lines were also observed near a reciprocal-lattice point and the incident beam (000 reflection) for a thick enough crystal. Very recently, Kashiwase *et al.*<sup>11</sup> have briefly reported on the excess diffraction line in detail using monochromatized synchrotron radiation and a triple-crystal diffractometer with both collimator and analyzer made of grooved silicon crystals. They clearly demonstrated that the intensity peak was caused by the anomalous transmission of TDS, consistent with the patterns predicted qualitatively.<sup>10</sup> However, a quantitative analysis of the experimental intensity profile of the peak was not made at that time.

In the Bragg (reflection) geometry of perfect crystals, Eisenberger, Alexandropoulos, and Platzman<sup>12</sup> and Iida and Kohra<sup>13</sup> succeeded in observing acoustic phonons with very small momenta in perfect crystals. Spalt *et al.*<sup>14</sup> observed interference effects when coherently coupled x-ray beams are inelastically scattered by phonons in a silicon crystal. Apart from a difference in Laue and Bragg geometries, their observation<sup>14</sup> is complementary to the present report, and they have tried to explain the phenomena as interference of TDS x rays subsequent to Bragg reflections in a perfect crystal. The diffraction profile in a true reciprocal process of the present work has been observed using monochromatized synchrotron radiation.<sup>15</sup>



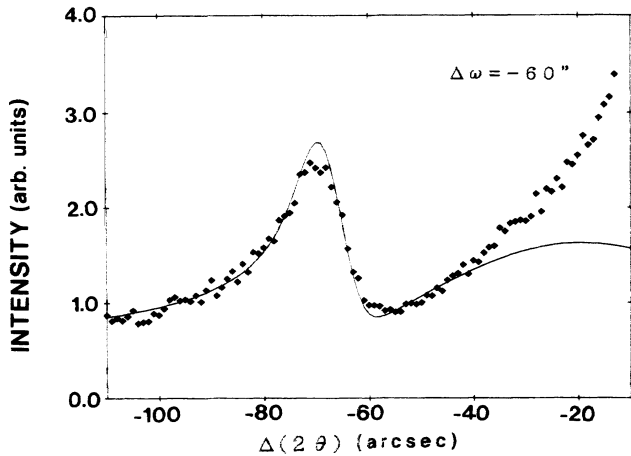


FIG. 3. Observed (marked) and convoluted (solid line) intensity profile of TDS including the diffraction peak corresponding the excess line across the  $\bar{2}\bar{2}0$  TDS for the same condition as in Fig. 4. As the central angle of the peak profile is taken to be a fitting parameter, the absolute value of peak position is meaningless.

measurement of the rocking curves of the  $\bar{2}\bar{2}0$  reflection in the Laue geometry. Each observed rocking curve had a symmetric profile with a full width at half maximum (FWHM) of 5.6 and 7.5 arc sec, which are both very close to the theoretical values for absorbing perfect germanium crystals.

To obtain the intensity profile of the  $\bar{2}\bar{2}0$  TDS in which an excess line is expected to appear as a peak, an angle-resolved measurement was made across the TDS by rotating the analyzer crystal stepwise with the specimen crystal fixed near the  $\bar{2}\bar{2}0$  Bragg reflection point. Scattering due to surface imperfection and roughness can be disregarded in the intensity measurements, since all scattering except for the anomalous transmission is strongly absorbed in penetrating the specimen crystal. The intensity is normalized by ionization chamber (IC) currents of the incident beam. The direction of the scattered x rays was determined by the rotation angle of the analyzer. The angle  $\Delta(2\theta)$  indicates the angular deviation of the analyzer from the maximum-intensity angle of the  $\bar{2}\bar{2}0$  Bragg peak when the specimen is just on the Bragg position. The angle  $\Delta(2\theta)$  was taken to be positive for increasing scattering angle  $2\theta$ . In practice, in the Laue geometry  $\Delta(2\theta) = 2\theta - 2\theta_B = \Delta\theta + \Delta\omega$  to a good approximation. Here,  $\Delta\theta$  does not signify one-half of  $\Delta(2\theta)$ , but indicates, as shown in Fig. 2(a), the difference between the  $\bar{2}\bar{2}0$  reflecting plane and propagation direction

of the transmitted TDS waves on the exit surface of the crystal. The crystal orientation was indicated by the angular deviation  $\Delta\omega$  from the maximum-intensity position of the  $\bar{2}\bar{2}0$  Bragg peak.

To obtain the profile of TDS in which a diffraction line was expected, constant step scanning of the analyzer (scattering angle) was made with the specimen crystal fixed near the  $\bar{2}\bar{2}0$  Bragg position. The square symbols in Fig. 3 show an example of the observed diffraction-peak profile of TDS plotted against the scattering angle  $\Delta(2\theta)$  for  $\Delta\omega = -60$  arc sec. (The experimental results on absorption and angular dependences are shown in Figs. 5 and 6, where the intensity is taken to be in relative scale.)

### III. THEORY

The experimental results are now compared with a calculation according to the treatment based on the dynamical theory given by Kashiwase *et al.*<sup>10</sup> We consider the propagation of incident and TDS x-ray waves in the symmetric Laue geometry of a parallel-plate crystal of thickness  $D$ , as shown in Figs. 2(a) and 2(b). A monochromatic parallel beam of wavelength  $\lambda$  and intensity  $I_0$  in  $\sigma$  polarization is incident on the  $(2\bar{2}0)$  plane at a glancing angle  $\theta_B + \Delta\omega$ , where  $\theta_B$  is the Bragg angle and  $\Delta\omega$  is the angular deviation of a crystal from  $\theta_B$ . The experiment was performed for  $20 < |\Delta\omega| < 180$  arc sec, which is much smaller than  $\theta_B$ , but larger than the incident-beam divergence and FWHM of the  $\bar{2}\bar{2}0$  Bragg reflection. The incident beam is attenuated first by ordinary absorption during propagation, with no Bragg reflection, from the entrance surface to the depth  $t$  in the crystal; at this depth, one-phonon scattering, i.e., TDS, occurs in the layer  $t - t + \Delta t$  into a direction near the  $\bar{2}\bar{2}0$  reflection. A part of the TDS, impinging on the  $(\bar{2}\bar{2}0)$  plane at nearly the Bragg angle  $\theta_B$ , excites the Bragg reflection. In a narrow angular region  $|\Delta\theta| < \Delta\theta_B$  comparable with the FWHM  $2\Delta\theta_B$ , where the  $\bar{2}\bar{2}0$  Bragg reflection is strongly excited, the transmitted and reflected TDS waves interact dynamically to form two waves which are strongly or weakly absorbed according to whether they have antinodes or nodes on the reflecting atom planes. This causes an anomalous absorption or transmission, well known as the Borrmann effect.<sup>17</sup> The wave with nodes at the atom planes propagates through the crystal of thickness  $D-t$  below  $t$  with anomalously low absorption. Emerging from the exit surface of the crystal, the transmitted and reflected TDS waves will be observed near the TDS and incident spots, respectively.

The transmitted intensity  $\Delta I_{hT}$  from the layer  $\Delta t$  is given by

$$\Delta I_{hT} = I_0 \exp(-\mu t / \gamma) S_h \Delta t / D \frac{1}{2} \left\{ \frac{1}{2} \left[ 1 - \frac{W}{(1+W^2)^{1/2}} \right]^2 \exp \left[ -\frac{\mu}{\gamma} (D-t) \left[ 1 - \frac{K_0}{(1+W^2)^{1/2}} \right] \right] + \frac{1}{2} \left[ 1 + \frac{W}{(1+W^2)^{1/2}} \right]^2 \exp \left[ -\frac{\mu}{\gamma} (D-t) \left[ 1 + \frac{K_0}{(1+W^2)^{1/2}} \right] \right] \right\}, \quad (1)$$

with the normal x-ray linear absorption coefficient  $\mu$  and  $\gamma = \cos(\theta_B + \Delta\omega) \cong \cos(\theta_B)$ . Here

$$K_0 = (\phi_{hi} / \phi_{oi})(|\phi_{hr}| / \phi_{hr}) \quad (2)$$

and

$$W = \Delta\theta \sin(2\theta_B) / |\phi_{hr}|, \quad (3)$$

where  $\phi_{hr}$ ,  $\phi_{hi}$ , and  $\phi_{oi}$  are the real and imaginary parts of the  $\mathbf{h}=(2,2,0)$  and  $(0,0,0)$  Fourier coefficients  $\phi_{\mathbf{h}}, \phi_0$  of the complex electric susceptibility of the germanium crystal and  $\phi_{\mathbf{h}} = (e^2/mc^2)\lambda^2 F_{\mathbf{h}} / (\pi v_a)$ . Here  $v_a$  is the unit cell volume,  $F_{\mathbf{h}}$  is the structure factor of index  $\mathbf{h}$  corrected with a temperature factor, and its real part is denoted by  $F_{hr}$ . (In this paper we consider only a crystal with inversion symmetry.) The parameter  $\Delta\theta$  is the difference angle shown in Fig. 2(a). The factor  $S_{\mathbf{h}}$  is the intensity of TDS per unit incident x-ray intensity. In the long-wavelength acoustic approximation based on kinematical first-order TDS theory,  $S_{\mathbf{h}}$  is given as

$$S_{\mathbf{h}} = k_B T |F_{hr}|^2 [\mathbf{b} \cdot \vec{\Omega}^{-1} \cdot \mathbf{b}] \delta V / (v_a^2 q^2), \quad (4)$$

with  $\mathbf{b} = \mathbf{K}'_{\mathbf{h}} - \mathbf{K}_0 = \mathbf{h} + \mathbf{q}$ . Here  $\mathbf{K}_0$ ,  $\mathbf{K}'_{\mathbf{h}}$ , and  $\mathbf{q}$ , respectively, are the wave vectors of the incident and TDS x rays and phonon wave in the crystal, and  $\delta V$  is the scattering volume of the specimen. The tensor  $\vec{\Omega}^{-1}$  is the inverse tensor of  $\vec{\Omega}$  and is dependent on the direction of  $q$  and the elastic constants of the crystal (for details, see Ref. 18).

Integration of Eq. (1) leads to total transmitted TDS intensity

$$I_{hT} = I_0 S_{\mathbf{h}} J_{hT}, \quad (5)$$

with

$$J_{hT} = \frac{\gamma(1+W^2)^{1/2}}{D \Delta\mu} \exp(-\mu D / \gamma) \times \left\{ \left[ 1 - \frac{1}{2(1+W^2)} \right] \sinh \left[ \frac{D \Delta\mu}{\gamma(1+W^2)^{1/2}} \right] - \frac{W}{(1+W^2)^{1/2}} \left[ \cosh \left[ \frac{D \Delta\mu}{\gamma(1+W^2)^{1/2}} \right] - 1 \right] \right\}, \quad (6)$$

where  $\Delta\mu = K_0 \mu$ .

In the present theoretical treatment, only the dynamical Bragg reflection of TDS near the  $[2\bar{2}0]$  direction is taken into account. Strictly, we should consider the intensity  $S_0$  due to the Bragg reflection of TDS near the 000 direction and, further, an interference term associated with the true TDS waves. In the present case, such effects may be negligibly small in comparison with  $I_{hT}$ , since  $S_0$  [TDS of  $\mathbf{h}=(0,0,0)$ ]  $\ll S_{\mathbf{h}}$  [TDS of  $\mathbf{h}=(2,-2,0)$ ]. Finally, the intensity formula for the diffraction-peak profile near the reciprocal-lattice point  $\mathbf{h}=(2,-2,0)$  can be expressed approximately by  $I_{hT}$ .

#### IV. COMPARISON BETWEEN EXPERIMENTAL AND CALCULATED RESULTS

The intensity profile of the TDS diffraction peak was calculated as follows to compare with the experimental results. The momentum vector of the phonon, needed for calculating  $S_{\mathbf{h}}$ , was determined by the scattering angle  $2\theta$  and the offset angle  $\Delta\omega$ . The solid and dotted curves in Fig. 4(a) show profiles of  $J_{hT}$  and  $S_{\mathbf{h}}$ , respectively, calculated from Eqs. (6) and (4) in the case of  $\Delta\omega = -60$  arc sec for the  $2\bar{2}0$  reflection of a germanium specimen of thickness  $D=0.10$  mm. Figure 4(b) shows that the shape of the profile  $I_{hT}$  is similar to the experimental result in Fig. 3, although the calculated peak is narrower because of neglect of the experimental resolution. In the calculation, fitting of the intensity profile near  $\Delta(2\theta)=0$  was not tried, since the peak near  $\Delta(2\theta)=0$  is explained primarily as the tail of  $2\bar{2}0$  Bragg reflection, and we are interested only in the dynamical diffraction of TDS x rays.

The intensity profile of the diffraction peak calculated by Eqs. (4) and (6) should be compared with experiment after performing a convolution to account for the reflection widths of monochromator, collimator, and analyzer. To make the calculation simple, we assume as follows: (1) The incident radiation is monochromatic of wavelength 1.540 Å from an ideally distant point source; we neglect *finite angular and energy widths* scattered dynamically by the monochromator. (2) The reflectance (resolution) function of the collimator and analyzer of

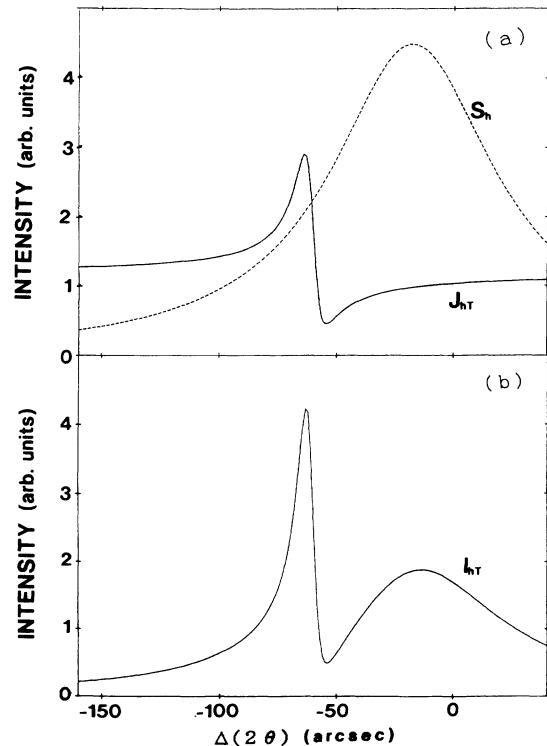


FIG. 4. (a) Solid and dotted curves are the calculated profiles of  $J_{hT}$  and  $S_{\mathbf{h}}$  in Eq. (5), respectively, at  $\Delta\omega = -60$  arc sec for the germanium  $2\bar{2}0$  reflection and thickness  $D=0.10$  mm. (b) The calculated profile of  $I_{hT}$ .

TABLE II. Elastic constant values used for the calculation of  $S_h$ .

$C_{11}$	$C_{12}$	$C_{44}$
12.89 ( $10^{11}$ dyn/cm <sup>2</sup> )	4.83 ( $10^{11}$ dyn/cm <sup>2</sup> )	6.71 ( $10^{11}$ dyn/cm <sup>2</sup> )

grooved silicon crystals, being *tailless* by virtue of five consecutive symmetric 220 Bragg reflections, is approximated simply as

$$C(x) = \begin{cases} 0, & |x| > \Delta\theta_M, \\ \text{const}, & |x| < \Delta\theta_M, \end{cases} \quad (7)$$

where  $2\Delta\theta_M$  is the theoretical angular FWHM of the Si 220 Bragg reflection. Here we neglected the energy and spatial divergence of the x rays passing through the monochromator. The intensity distribution  $I_{\text{calc}}(x)$  of a diffraction-peak profile was then expressed as double convolutions of  $C(x)$  and the theoretical intensity distribution  $I_{hT}$  in Eq. (5). Then we have

$$I_{\text{calc}}(x) = \int \int C(x-u) I_{hT}(v) C(u-v) dv du, \quad (8)$$

where  $x$  is given by  $\Delta\theta$  or  $\Delta(2\theta)$ .

Test rocking profiles of the  $\bar{2}20$  Bragg reflections were found to be in excellent agreement with the profiles calcu-

lated by Eq. (8), in spite of the above simplification that x-ray energy and angular divergences of the monochromator and angular dependence of the collimator (analyzer) reflectance could be all ignored. Therefore Eq. (8) is applicable to calculating diffraction profiles. We finally had two important fitting parameters for each specimen: background and reflectance of the collimator or analyzer. Numerical calculation of the intensity profile of the diffraction peak was carried out to compare with the experimental result by using Eq. (8) and the values in Table II. Even the thinner specimen *A* was thick enough to cause dynamical diffraction and absorption in comparison with the extinction distance  $7.2 \mu\text{m}$  and  $\mu D = 3.5$  for the  $\bar{2}20$  reflection of the  $1.540\text{-\AA}$  x ray. The solid line in Fig. 3 shows the convoluted intensity profile  $I_{\text{calc}}$  of the diffraction peak for specimen *A*. Figure 3 shows good agreement between the experimental and calculated profiles, except the part of the peak near  $\Delta(2\theta) = 0$ . The peak of specimen *A* is composed of

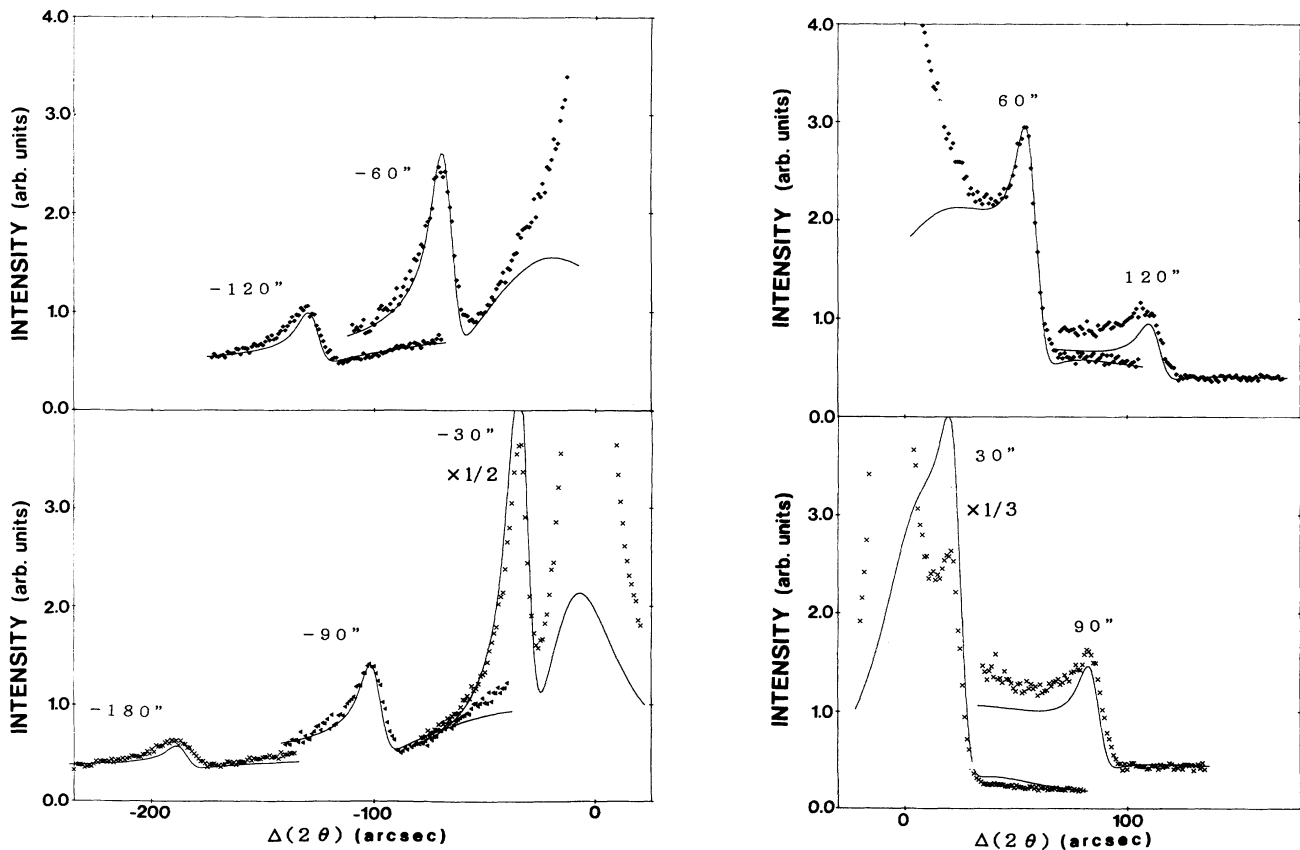


FIG. 5. Observed (marked) and calculated (solid line) intensity profiles of diffraction peaks corresponding to the excess-deficit lines across  $\bar{2}20$  TDS of specimen *A* with thickness 0.10 mm for various offset angles  $\Delta\omega = -180, -120, -90, -60, -30, 30, 60, 90$ , and  $120$  arc sec. Intensity profiles for the offset angles  $\Delta\omega = -30$  and  $30$  arc sec are shown after a reduction by a factor of 2 and 3 in intensity scale, respectively. Extra peaks near  $\Delta(2\theta) = 0$  are from the tail of the 220 Bragg reflection.

strongly excess and weakly deficit parts, as shown theoretically as the solid line of Fig. 4(a). As this curve is determined by a specimen thickness, Fig. 4(a) also shows that the excess part is on the lower angle side and the deficit is on the higher. In this asymmetry an excess part always appears at a scattering angle lower than a deficit part. As already mentioned, for simplicity we are not concerned with the intensity profile of the  $\Delta(2\theta)=0$  peak, which is influenced by the tail of the  $2\bar{2}0$  main Bragg peak.

The fitting calculation was carried out for several offset angles  $\Delta\omega$  and specimen thicknesses  $D$ , and we added the central angle of the diffraction profile where  $\Delta(2\theta)=0$  as one more fitting parameters. Therefore the absolute value of the peak position is meaningless, and only the relative value is meaningful. Figures 5 and 6 show the convoluted theoretical curves (solid line) and experimental curve (marked) for several offset angles of specimens  $A$  and  $B$ . All profiles show good agreement in theory and experiment. They also show that the profile of the diffraction peak mainly depends on the specimen thickness ( $\mu D$ ), and its peak intensity depends on the offset an-

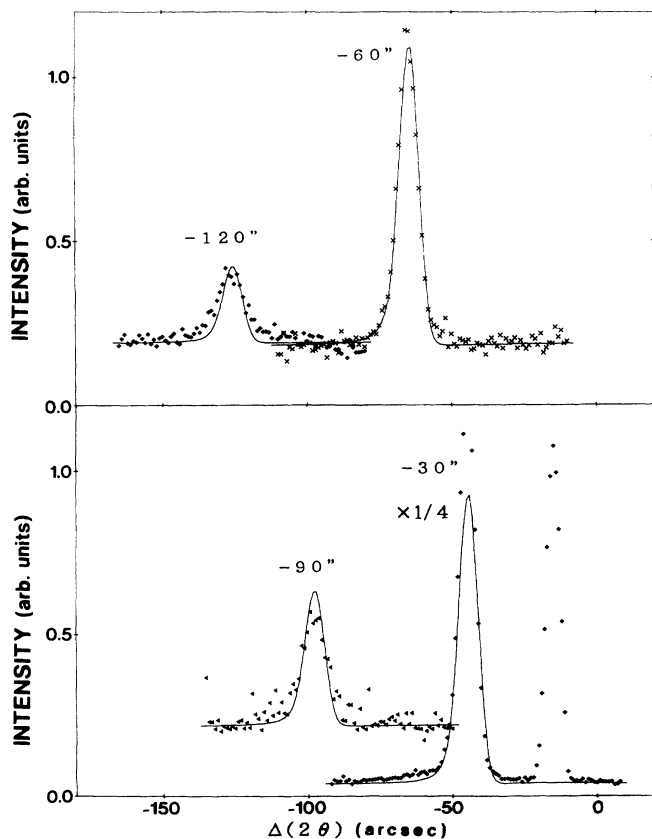


FIG. 6. Observed (marked) and calculated (solid line) intensity profiles of diffraction peaks corresponding to the excess lines across the  $2\bar{2}0$  TDS of specimen  $B$  with thickness 0.25 mm for various offset angles  $\Delta\omega = -120$ ,  $-90$ ,  $-60$ , and  $-30$  arcsec. The intensity profile for the offset angle  $\Delta\omega = -30$  arcsec is shown after a reduction by a factor of 4 in intensity scale. One extra peak in the observed profile of  $\Delta\omega = -30$  arcsec is the peak due to the tail of the  $2\bar{2}0$  Bragg reflection.

gle. Decrease of the specimen thickness leads to increase of the peak intensity and the base (TDS) intensity. In addition, it causes a more asymmetric profile which appears as the excess-deficit line. In accordance with increase of the thickness, the diffraction peak becomes more symmetric since it is formed by a part of the TDS x rays anomalously transmitted with little absorption. Two slight disagreements between the calculation and experimental points are described: the offset-angle dependence of the experimental peak intensity is less than that of the calculated (TDS) intensity, and its peak width becomes broader than the calculated width with higher offset angles.

We treated the value of specimen thickness  $D$  as a fitting parameter, and the error of thickness was estimated to be 15% of each. Both the value of the specimen thickness and its error value were nearly equal to those obtained in a thickness measurement of the specimen.

## V. SUMMARY AND DISCUSSION

A high-angular-resolution measurement of sharp diffraction-peak profiles in the  $2\bar{2}0$  TDS in the transmission Laue geometry for perfect germanium crystals has been performed by means of monochromatized synchrotron radiation and a triple-crystal diffractometry system. Quantitative comparisons with theoretical profiles were made on the basis of the dynamical diffraction theory including absorption. The effect of reflectance of the collimator and analyzer was also taken into account with some simplifications. As described in our earlier Letter,<sup>11</sup> the observed angle of the diffraction-peak position is nearly equal to the offset angle  $\Delta\omega$ . The result of this study is summarized in the following.

(1) The intensity profile of each diffraction peak, which depends strongly on the offset angle  $\Delta\omega$ , is in good agreement with the calculation of the above-mentioned model. Therefore the main origin of the diffraction peak is confirmed quantitatively to be in the dynamical anomalous transmission of TDS x rays in the absorbing perfect crystal.

(2) The intensity profile of the diffraction peak varies from excess-deficit to excess as the specimen thickness increases. The thickness dependence in the calculated intensity profile explains the experimental result.

(3) The intensity profile of the diffraction peak of the thinner specimen  $A$  is asymmetric with a excess-deficit line.<sup>10</sup> The deficit part in the excess-deficit intensity profile appears at a scattering angle slightly higher than the excess part, which is independent of the sign of the offset angle  $\Delta\omega$ .

Both calculated and experimental profiles are in excellent agreement for all offset angles and specimen thicknesses. Two slight disagreement points should, however, be noted: The dependence of the experimental peak intensity on the offset angle is less than that of the calculated (TDS) intensity, and the peak width becomes broader than the calculated width for the higher offset angle. The former is understandable since the measured x rays may contain scattered x-ray components having weaker  $q$  dependence than the TDS x ray. Some (inelas-

tic) x rays from the specimen, reflected by the analyzer, at slightly different angles from the TDS x-ray direction, may enter the detector because we did not use sharp slits before the analyzer and we adopted the (+, -) arrangement for the specimen and analyzer system, as shown in Fig. 1. Next, the diffraction-peak broadening in appearance can be explained. The angular deviation of the diffraction-peak direction due to the inelastic x rays of other origins almost compensates for the angular deviation of the scattering direction from the analyzer, and the (inelastic) x-ray direction to the detector then becomes nearly equal to the TDS x rays. These x rays may be fluorescent, scattered by air, or due to Compton scattering, and we may briefly think about which of these are important here. The origin of the wider peak width is considered due to the weak intensity profile, having a peak position shifted a very little (order of seconds), being added to the intensity profile of the TDS. Fluorescent x rays are ineffective, as the wavelength is too different from the incident 1.540-Å x rays. As for the contribution of Compton x rays, the x rays scattered directly into the direction of  $I_{hT}$  ( $2\theta_B$ ) have an energy difference of about 10 eV compared with the incident x ray, and this is not reflected by the analyzer. But the Bragg reflected x rays

of small-angle Compton scattering ( $\sim 60$  arc sec) have a quasielastic energy difference of only the order of  $\mu\text{eV}$ . The origin of the profile broadening is then probably explained by adding Bragg reflected x rays of small-angle Compton scattering, air scattering, and multiphonon-scattered x rays to the intensity profile of the TDS x ray.

Finally, the origin of the two disagreement points may also arise in the undetermined error in phonon momentum caused by the extinction distance and the component of the momentum perpendicular to the normals of the Bragg reflecting planes. A further experiment would be necessary to determine the actual source of profile broadening using sharp slits to confine more accurately the scattering direction from the specimen.

#### ACKNOWLEDGMENTS

The authors are indebted to Dr. S. C. Moss, University of Houston, for a critical reading of this manuscript. They thank the Photon Factory Program Advisory Committee for granting access to their facility. The authors express their sincere thanks to Dr. Y. Hirose of Fundamental Research Laboratories, NEC Co. Ltd., for his advice.

\*Present address: Department of Applied Physics, Faculty of Engineering, The University of Tokyo, Bunkyo, Tokyo 113, Japan.

†Present address: Research Laboratory of Engineering Materials, Tokyo Institute of Technology, Midori, Yokohama 227, Japan.

<sup>1</sup>Y. Kashiwase, Y. Kainuma, and M. Monoura, *J. Phys. Soc. Jpn.* **50**, 2793 (1981); *Acta Crystallogr. A* **38**, 390 (1982).

<sup>2</sup>V. A. Bushuev, A. V. Laushkin, R. N. Kuz'min, and N. N. Lobanov, *Phys. Tverd. Tela (Leningrad)* **25**, 406 (1983) [*Sov. Phys. Solid State* **25**, 228 (1983)].

<sup>3</sup>V. A. Bushuev and A. G. Lyubimov, *Kristallografiya* **32**, 311 (1987) [*Sov. Phys. Crystallogr.* **32**, 179 (1987)].

<sup>4</sup>W. C. Hamilton, *Acta Crystallogr.* **10**, 629 (1957); W. H. Zachariasen, *ibid.* **23**, 558 (1967).

<sup>5</sup>Y. Oya and Y. Kashiwase, *J. Phys. Soc. Jpn.* **57**, 2026 (1988).

<sup>6</sup>M. Mori, Y. Kashiwase, M. Kogiso, and S. Sasaki, *Acta Crystallogr. A* **46**, 923 (1990).

<sup>7</sup>Y. Kainuma, *J. Phys. Soc. Jpn.* **16**, 228 (1961); *Acta Crystallogr.* **8**, 247 (1955).

<sup>8</sup>Y. Kashiwase and Y. Kainuma, *J. Phys. Soc. Jpn.* **51**, 2379 (1982); **53**, 3438 (1984).

<sup>9</sup>Y. Kashiwase, M. Mori, M. Kogiso, M. Minoura, S. Sasaki, and T. Ishikawa, *J. Phys. Soc. Jpn.* **55**, 4172 (1986).

<sup>10</sup>Y. Kashiwase, M. Mori, M. Kogiso, M. Minoura, and S. Sasaki, *J. Phys. Soc. Jpn.* **57**, 524 (1988).

<sup>11</sup>Y. Kashiwase, M. Mori, M. Kogiso, K. Ushida, M. Monoura, T. Ishikawa, and S. Sasaki, *Phys. Rev. Lett.* **62**, 925 (1989).

<sup>12</sup>P. Eisenberger, N. G. Alexandropoulos, and P. M. Platzman, *Phys. Rev. Lett.* **23**, 1519 (1972).

<sup>13</sup>A. Iida and K. Kohra, *Phys. Status Solidi A* **51**, 533 (1979).

<sup>14</sup>H. Spalt, A. Zounek, B. N. Dev, and G. Materlik, *Phys. Rev. Lett.* **60**, 1868 (1988).

<sup>15</sup>Y. Kashiwase, M. Kogiso, M. Mori, M. Minoura, T. Ishikawa, and X. Zhang, *J. Phys. Soc. Jpn.* **60**, 2554 (1991).

<sup>16</sup>T. Ishikawa, J. Matsui, and T. Kitano, *Nucl. Instrum. Methods A* **246**, 613 (1986).

<sup>17</sup>G. Borrmann, *Z. Phys.* **42**, 157 (1941).

<sup>18</sup>For example, W. H. Zachariasen, *Theory of X-Ray Diffraction in Crystals* (Dover, New York, 1967), Chap. 4.7.